A triple decomposition of the fluctuating motion below laboratory wind water waves

Laurent Thais and Jacques Magnaudet

Institut de Mécanique des Fluides de Toulouse, Unité de Recherche Associée au CNRS, Toulouse, France

Abstract. Understanding of the dynamics of the top meters of the ocean requires an improvement of present knowledge about interactions between wind waves, mean sheared current, and turbulence. To achieve this goal, a key point lies in relevant definitions and evaluations of orbital and turbulent motions. The aim of this paper is to build and validate a separation technique allowing one to distinguish all three crucial contributions of the fluctuating motion, namely the potential and rotational parts of the orbital motion, as well as turbulent fluctuations. The whole method is first developed and tested for periodic rotational waves. The first step of this technique consists of a determination of the instantaneous stream function associated with the potential motion induced by the waves in presence of a linear sheared current. The second step consists of a linear filtration of the remaining motion from which the orbital rotational motion is extracted. The strong hypotheses involved in the technique are then carefully checked and shown to be relevant in the case of laboratory wind waves. The method is finally applied to experimental data obtained by laser Doppler velocimetry measurements in a wind-water laboratory facility. Influence of the mean sheared current on the prediction of orbital velocities is pointed out, and the orbital rotational contribution is found to have a significant magnitude.

1. Introduction

When wind blows over a water surface initially at rest, it creates a pattern of random gravity waves. Study of surface waves is usually performed within the framework of classical potential theory which experiences largely success in describing many observed phenomena. However, it has been suspected for a long time that in the presence of wind the assumption of irrotationality is only approximately valid. The pioneering field measurements of *Shonting* [1964, 1970], *Yefimov and Khristoforov* [1971a, b], and *Cavaleri et al.* [1978] showed that the phases of the orbital velocity components measured with respect to the wave elevation deviate significantly from linear theory predictions. Things appeared even clearer some years later in two remarkable series of experiments. In the first one, *Cavaleri and Zecchetto* [1987] performed measurements in the Adriatic Sea near Venice and confirmed unambiguously that the phase shift between horizontal velocity fluctuation and wave elevation is far from being zero in presence of wind leading to important downward momentum fluxes. In contrast, the same authors observed that under swell conditions the results were coherent with the predictions of the classical theory. *Cheung* [1985] and *Cheung and Street* [1988a] confirmed the existence of an orbital vorticity by using sinusoidal, mechanically generated waves ruffled by a slight wind; they observed the existence of an orbital shear stress of the same order as the surface stress. In the same investigation they noted an abnormally high turbulence level below the waves (between three and four times the level in a classical boundary layer), and it seems obvious that both features are closely related. Another proof of the departure of wind waves from irrotationality is the development of Langmuir circulations. It was shown by *Craik and Leibovich* [1976] (see also *Leibovich* [1983] for a review) that the interaction between an initially irrotational surface wave field and a wind-driven current leads to the existence of a weak vorticity correlated to the wave motion and can explain the occurence of quasi-steady vortices aligned with the wind direction.

All these results appear as converging indications of the existence of an orbital vorticity below waves when wind is present. Even weak, this vorticity is able to change dramatically the mean momentum balance (as is shown by the existence of Langmuir circulations) or the turbulence balance (as it appeared in the results of *Cheung and Street* [1988a]). This is due to the fact that wave energy is generally much greater than energies associated with mean current or turbulence, so that any departure from the potential behavior can have very strong consequences. It is thus clear that understanding and description of the orbital rotational motion is an essential point for the determination of fluxes at the atmosphere-ocean interface, as well as for the knowledge of small-scale dynamics of the surface layer in lakes and oceans.

When dealing with experimental results, the central problem is then to build a method allowing extraction from any velocity measurement of the orbital potential and rotational contributions. Things would be relatively easy if the fluctuating motion below wind waves was restricted to the orbital motion. Unfortunately, this flow is known to be turbulent, even at very weak wind speeds. The major problem of signal processing is then to separate two random orbital motions out of a random fluctuation containing a turbulent contribution. Many attempts have been made to perform this kind of separation between an orbital and a turbulent motion, but two methods seem to emerge as the most powerful. They both require the simultaneous measurement of wave elevation and velocity at the same fetch.

Paper number 94JC02714.
0148-0227/95/94JC-02714$05.00

The first method derived by *Benilov and Filyushkin* [1970] is called the linear filtration technique (hereinafter referred to as LFT). In this method, which works in the frequency domain, the orbital motion is assumed to be linearly related to the surface displacement via a convolution process, while turbulence and orbital motion are assumed to be uncorrelated at first order.

The second method derived by *Dean* [1965] and updated by *Jiang et al.* [1990] is a nonlinear least squares resolution in the time domain of the full kinematic and dynamic equations written at the free surface. It assumes that the orbital motion is two-dimensional and potential.

The aim of the present paper is to present a somewhat more general separation method enabling us to estimate the orbital rotational motion below laboratory wind waves, as well as the orbital potential motion and the turbulent contribution. This method is based on the following remark: since LFT allows the orbital motion to carry vorticity when the *Dean* [1965] method does not, it appears theoretically possible to combine both of these methods to obtain separately all three contributions. Nevertheless, as the propagation of wind waves is greatly affected by the wind-induced mean current, it is not possible to compute accurately the orbital motion without taking into account the main characteristics of this current. Thus it is first necessary to reconsider the Dean method so as to adapt it to random waves propagating on a sheared current. Furthermore, since the orbital rotational contribution is a priori much smaller than its potential counterpart, its determination requires a very careful discussion of the hypotheses and the limits of each step of the procedure. This discussion and the tests presented below show that under suitable conditions fulfilled in laboratory experiments the present method gives a reliable estimation of the orbital rotational effects. It is then possible to use experimental data to compute various correlations crucial for the understanding of wave-current and wave-turbulence interactions. On the basis of these correlations a physical analysis of these interactions is presented in a companion paper [*Magnaudet and Thais*, this issue] (hereinafter referred to as MT).

2. Foundations of the Method: Two-Dimensional Periodic Waves

2.1. Triple Decomposition of the Fluctuating Motion

As previously explained, our goal is to devise a method allowing a physical analysis of the velocity field below laboratory wind waves. For the sake of clarity it seems necessary to explain and check the method first with two-dimensional periodic waves, then to discuss its extension to wind-generated waves. Consequently, in this section we consider the case of two-dimensional periodic waves superimposed on a turbulent shear flow. This physical situation is encountered, for example, when waves are generated by means of a wave maker while a slight wind blows over the surface.

The total fluctuating velocity $\mathbf{v}$ measured below the waves can be regarded as the sum of the turbulent motion $\mathbf{v}'$ and the orbital motion $\tilde{\mathbf{v}}$. We define $\tilde{\mathbf{v}}$ using the phase-averaging method proposed by *Reynolds and Hussain* [1972]. Denoting the wave period T and its phase θ with respect to an arbitrary time, the phase-averaged contribution contained into the instantaneous velocity field $\mathbf{V}$ is defined as

$$<\mathbf{V}>(\mathbf{x},\theta)=\frac{1}{N_w}\sum_{n=1}^{N_w}\mathbf{V}(\mathbf{x},\theta+nT) \tag{1}$$

where N_w is the number of available wave groups, assumed to be large. The mean velocity $\overline{\mathbf{V}}$ is obtained from (1) by integrating $<\mathbf{V}>$ along θ as

$$\overline{\mathbf{V}}(\mathbf{x})=\frac{1}{2\pi}\int_0^{2\pi}<\mathbf{V}>(\mathbf{x},\theta)\,d\theta \tag{2}$$

The orbital velocity $\tilde{\mathbf{v}}$ is finally given by

$$\tilde{\mathbf{v}}(\mathbf{x},\theta)=<\mathbf{V}>(\mathbf{x},\theta)-\overline{\mathbf{V}}(\mathbf{x}) \tag{3}$$

The turbulent contribution $\mathbf{v}'$ is simply the nonperiodic part of $\mathbf{V}$. This definition implies that no phase correlation can exist between $\mathbf{v}'$ and the wave elevation η, so that

$$\overline{\mathbf{v}'\eta}=0 \tag{4}$$

Equation (4) does not mean that turbulent fluctuations are not affected by waves; phase correlation can occur between wave elevation and higher-order turbulent quantities like the Reynolds stresses $<\mathbf{v}'\mathbf{v}'>$ (defined by applying the phase average procedure to the tensor $\mathbf{v}'\mathbf{v}'$).

Since the experimental and theoretical studies reviewed in the Introduction have shown the orbital rotational motion to be of particular interest, the orbital motion is split in two parts as

$$\tilde{\mathbf{v}}(\mathbf{x},\theta)=\tilde{\mathbf{v}}_P(\mathbf{x},\theta)+\tilde{\mathbf{v}}_R(\mathbf{x},\theta) \tag{5}$$

where $\tilde{\mathbf{v}}_P$ and $\tilde{\mathbf{v}}_R$ denote respectively the potential and rotational contributions to $\tilde{\mathbf{v}}$. Note that (5), which expresses the Helmholtz decomposition of $\tilde{\mathbf{v}}$, does not define in a unique way $\tilde{\mathbf{v}}_P$ and $\tilde{\mathbf{v}}_R$ since an arbitrary gradient can be added to $\tilde{\mathbf{v}}_P$ and substracted from $\tilde{\mathbf{v}}_R$. This ambiguity will be removed in the following subsection.

Combining previous decompositions, the total fluctuating water motion $\mathbf{v}$ measured as a function of time t can finally be written as

$$\mathbf{v}(\mathbf{x},t)=\tilde{\mathbf{v}}_P(\mathbf{x},\theta)+\tilde{\mathbf{v}}_R(\mathbf{x},\theta)+\mathbf{v}'(\mathbf{x},t) \tag{6}$$

The general problem we have in mind is now to obtain a reliable estimate of $\tilde{\mathbf{v}}_P$, $\tilde{\mathbf{v}}_R$ and $\mathbf{v}'$.

2.2. Governing Equations of the Orbital Motion

Let us denote by $<\omega>$ and ω' the vorticities associated with $<\mathbf{V}>$ and $\mathbf{v}'$, respectively. The momentum balance of $<\mathbf{V}>$ is given in the inviscid limit by

$$\frac{\partial<\mathbf{V}>}{\partial t}+\nabla\left(\frac{<\mathbf{V}>^2}{2}+\frac{<\mathbf{v}'^2>}{2}+\frac{<P>}{\rho}+gz\right)+<\omega>\times<\mathbf{V}>+<\omega'\times\mathbf{v}'>=0 \tag{7}$$

where z is the vertical coordinate directed upward, while g and P denote gravity and pressure, respectively.

Obviously, in the frame of reference moving with the phase speed c of the periodic wave, the time derivative of $<\mathbf{V}>$

vanishes. The free surface then becomes a streamline, implying that the normal velocity (<V>-**c**).**n** is zero on this surface (**n** being the unit normal). Let us denote by **t** the unit vector tangent to <V> on the free surface, and by ds the arc element of this surface in the plane (**t**,**n**). Using the foregoing remarks, the momentum balance (7) integrated along ds on the surface leads to the Bernoulli equation

$$\frac{1}{2}(<\mathbf{V}>-\mathbf{c})^2+\frac{<v'^2>}{2}+\frac{<P>}{\rho}+g\eta + \int <\omega' \times \mathbf{v}'>.\mathbf{t}\, ds = constant \tag{8}$$

Assuming that the mean flow is also two-dimensional, the three parts of the phase-averaged motion can be written as

$$\overline{\mathbf{V}}-\mathbf{c}=-\mathbf{j}\times\nabla\overline{\Psi} \tag{9a}$$

$$\tilde{\mathbf{v}}_P=-\mathbf{j}\times\nabla\Psi_P \tag{9b}$$

$$\tilde{\mathbf{v}}_R=-\mathbf{j}\times\nabla\Psi_R \tag{9c}$$

where **j** is the unit vector defined so that (**t**, **n**, **j**) is right-handed. All three stream functions are related to the mean and orbital vorticities $\overline{\omega}$ and $\tilde{\omega}$ through

$$\nabla^2\overline{\Psi}=-\overline{\omega} \tag{10a}$$

$$\nabla^2\Psi_P=0 \tag{10b}$$

$$\nabla^2\Psi_R=-\tilde{\omega} \tag{10c}$$

On the free surface $z=\eta$, they also obey the kinematic and dynamic boundary conditions

$$\overline{\Psi}+\Psi_P+\Psi_R=\Psi_0 \tag{11}$$

$$\frac{1}{2}\left[\nabla(\overline{\Psi}+\Psi_P+\Psi_R)\right]^2+\frac{<v'^2>}{2}+\frac{<P>}{\rho}+g\eta + \int <\omega' \times \mathbf{v}'>.\mathbf{t}\, ds = gQ \tag{12}$$

where Ψ_0 and Q are two constants denoting the flow rate and the energy density of the total motion, respectively. Finally, at large depth the stream functions are assumed to satisfy the conditions

$$\overline{\Psi}-cz\rightarrow 0 \quad z\rightarrow -\infty \tag{13a}$$

$$\Psi_P\rightarrow 0 \quad z\rightarrow -\infty \tag{13b}$$

$$\Psi_R\rightarrow 0 \quad z\rightarrow -\infty \tag{13c}$$

At this point, it is necessary to stress that the orbital vorticity $\tilde{\omega}$ cannot generally be determined directly. Experimentally, its measurement looks extremely difficult to achieve with confidence, even though new techniques like digital particle image velocimetry (DPIV) [*Willert and Gharib*, 1991] give reasonable hope for estimating this quantity in future works. Another solution could be to solve numerically the coupled system (10)-(12) for a given wave record. This approach was used by *Thomas* [1990] to study the interactions between a mean sheared current and a periodic wave train. Unfortunately, the same way cannot be followed here because the generation of $\tilde{\omega}$ is due not only to mean current, but also to wave-turbulence interactions [*Magnaudet and Masbernat*, 1990]. Thus (10c) is of no use in the present framework, and the effects of the orbital vorticity have to be determined indirectly. Furthermore, (11)-(12) show that no rigorous separation exists between $\overline{\Psi}+\Psi_P$ and other quantities related to the orbital rotational motion or to the turbulent motion. In order to determine $\overline{\Psi}+\Psi_P$ without knowing $\tilde{\mathbf{v}}_R$ and **v**' on the surface, it must be assumed that the variations of Ψ_R, <P>, <v'^{2}> and <ω'xv'>.**t** along the surface are weak. This can be viewed as an asymptotic expansion of the total motion with respect to a small parameter representing the ratio between the magnitude of $\tilde{\mathbf{v}}_R+\mathbf{v}'$ and that of $\overline{\mathbf{V}}+\tilde{\mathbf{v}}_P$; in this expansion, $\overline{\Psi}+\Psi_P$ determines the unperturbed solution, whereas $\tilde{\mathbf{v}}_R$ and **v**' can be obtained at first order from the measured fluctuation **v** once $\tilde{\mathbf{v}}_P$ is known. Thus under the foregoing assumption $\overline{\Psi}$ and Ψ_P satisfy at leading order

$$\nabla^2\overline{\Psi}=-\overline{\omega} \tag{14a}$$

$$\nabla^2\Psi_P=0 \tag{14b}$$

$$\overline{\Psi}+\Psi_P=\Psi_1 \quad z=\eta \tag{15}$$

$$1/2g\left[\nabla(\overline{\Psi}+\Psi_P)\right]^2+\eta=Q_1 \quad z=\eta \tag{16}$$

$$\overline{\Psi}-cz\rightarrow 0 \quad z\rightarrow -\infty \tag{17a}$$

$$\Psi_P\rightarrow 0 \quad z\rightarrow -\infty \tag{17b}$$

From (15)-(16) there is no more ambiguity in the definition of $\tilde{\mathbf{v}}_P$ and $\tilde{\mathbf{v}}_R$; Ψ_P is now forced to satisfy conservation properties on a given free surface. Note that in (15)-(16) the constants Ψ_1 and Q_1 differ a priori from their counterparts, Ψ_0 and Q, which appear in (11)-(12); below waves, mass transport is known to be closely related to vorticity, so that the flow rate and the energy associated with the velocity field $\overline{\mathbf{V}}+\tilde{\mathbf{v}}_P$ are certainly different from those associated with the total phase averaged motion $<\mathbf{V}>=\overline{\mathbf{V}}+\tilde{\mathbf{v}}_P+\tilde{\mathbf{v}}_R$ even if $\tilde{\mathbf{v}}_R$ is weak. The total flow rate Ψ_0 is generally imposed by experimental conditions (for example, in a closed tank, $\Psi_0=0$). In contrast, as is well known in the study of Stokes waves on still water, Ψ_1 can have different values depending on the assumption made to fix Q_1. It is clear that this assumption can influence the absolute magnitude of $\tilde{\mathbf{v}}_R$. However, the most natural choice is guided by the fact that our primary aim is to device a method allowing treatment of experimental data. Since the surface elevation η is the key experimental data and since all velocity measurements are referred to the mean water level $\overline{\eta}$, it appears natural to define Q_1 and Ψ_1 so that $\overline{\eta}=0$. This definition will be used for the remainder of the present work.

2.3. Extraction of the Potential Contribution $\tilde{\mathbf{v}}_P$

Having defined the orbital potential motion by (15)-(17) and keeping in mind that our experimental data are η and the total velocity $\mathbf{v}+\overline{\mathbf{V}}$, we must first determine the "experimental" potential contribution $\tilde{\mathbf{v}}_P$. A powerful method to compute the potential motion induced by an experimentally known wave field composed of a sine wave and its harmonics was developed by *Dean* [1965]. Briefly, the method, assuming that the wave motion is two-dimensional, consists of a least squares determination of the Fourier components of a prescribed form of the stream function Ψ_P describing the orbital velocity field. The calculation is performed in the frame of reference $(x'=x-ct, z)$ moving with the constant phase velocity c of the wave train and Ψ_P is constrained to satisfy the full nonlinear kinematic and dynamic boundary conditions along the free surface. Ψ_P is assumed to be of the form

$$\Psi_P(x',z) = \sum_{n=1}^{N} \exp(nk_0 z)\,(X_{2n-1}\cos nk_0 x' + X_{2n}\sin nk_0 x') \qquad (18)$$

where k_0 is the wave number of the carrier wave and N the number of Fourier modes retained in the approximation. In his original work, *Dean* [1965] did not consider any mean current. In contrast, *Dalrymple* [1974] improved the method in order to take into account the effects of estuarine currents on surface waves. For this purpose, he introduced in (15)-(16) a stream function $\overline{\Psi}$ corresponding to a linear sheared current with known characteristics. However, the mean vorticity was weak and the overall effects of the current were small.

The situation is completely different here since the mean currents we are interested in are induced by the wind. These currents are known to influence greatly the characteristics of surface waves and especially the form of the dispersion relation (see, for example, *Thomas* [1979] and *Kirby and Chen* [1989]). In laboratory experiments the Eulerian surface drift ranges between 2 and 3% of the air free-stream velocity [*Phillips and Banner*, 1974 ; *Wu*, 1975] which corresponds frequently to 20 or 30% of the absolute phase velocity of young wind waves. Thus it appears that in presence of wind, no reliable estimation of $\tilde{\mathbf{v}}_P$ can be obtained without taking into account the current.

Possible forms of $\overline{\Psi}$ are restricted by the fact that the vorticity $\overline{\omega}$ must be constant for Ψ_P to satisfy (14b); according to the Rayleigh equation, this is the only case where the occurrence of a mean vorticity is compatible with a strictly potential orbital motion [*Peregrine*, 1976]. Taking into account this property, we consider a constant mean shear U_0' and assume:

$$\overline{\Psi}(z) = (c-U_0)\,z - U_0'\frac{z^2}{2} + C \qquad (19)$$

or in equivalent terms

$$\overline{U}(z) = U_0 + z\,U_0' \qquad (20)$$

In (19) the constant C is defined so that $\overline{\Psi}$ satisfy (17a) at large depth. It is clear that (20) does not describe the real wind-induced mean current over a large depth. However, this is not too serious of a problem because $\overline{\Psi}$ is only involved in the boundary conditions (15)-(16). What is necessary to obtain Ψ_P is simply an accurate approximation of the mean current within the surface region, so that $\overline{\Psi}$ only needs to be meaningful in that region. Nevertheless, it is not obvious to relate U_0 and U_0' to measurements for several reasons. The time-averaged, streamwise velocity that can be determined from a fixed point measurement at $z=0$ differs from the mean current because in this two-phase region the average of the orbital velocity differs from zero. The mean current which is measured below the two-phase region cannot be extrapolated up to $z=0$ because its vertical gradient is too strong. Thus it appears that only wave-following measurements can be easily related to U_0 and U_0'. A first idea would be to perform such measurements at various distances from the real free surface in order to average the results in the plane $z = 0$. This was done by *Cheung and Street* [1988b] for a mechanically generated periodic wave, but it appears as a very difficult technical challenge. The only wave-following measurement that can be easily performed is that of the Lagrangian surface drift U_l. This quantity is readily determined by measuring the time necessary for paper punchings dropped on the surface to travel a known distance and it can be shown (see appendix A) that if the mean current is assumed to decay linearly with depth, U_l can be expressed in terms of c, U_0, U_0', and wave-related quantities. More precisely, denoting by c_0 the relative phase velocity $c-U_0$, one finds for a sine wave of amplitude a and wave number k

$$U_l = U_0 + a^2k^2c_0 + a^2/2U_0'(2k + U_0'/c_0) \qquad (21)$$

Equation (21) closes the determination of $\tilde{\mathbf{v}}_P$. Once the wave elevation $\eta(x_0,t)$ is recorded at a given fetch x_0 and the absolute phase velocity c as well as the Lagrangian surface drift U_l are measured, $\overline{\Psi}+\Psi_P$ given by (18)-(19) and satisfying (21) can be determined. This is achieved by a least squares method whose constraints are equations (15)-(16), whereas the $2N+3$ unknowns are the Fourier coefficients X_n, the surface value Ψ_1 of the stream function, and the characteristics of the mean current U_0 (or in an equivalent way, c_0) and U_0'. Once this is realized, the resulting stream function $\overline{\Psi}+\Psi_P$ can be differentiated with respect to x' and z to obtain both components of $\tilde{\mathbf{v}}_P$. In the following, $\tilde{\mathbf{v}}_P$ will be often split into a linear part $\tilde{\mathbf{v}}_{P1}$ and a nonlinear part $\tilde{\mathbf{v}}_{P2}$. The linear orbital potential velocity $\tilde{\mathbf{v}}_{P1}$ is defined as the solution of the linearized form of (15)-(16) (see (B2)-(B3) in appendix B) applied to the same wave elevation η.

2.4. Extraction of the Rotational Contribution $\tilde{\mathbf{v}}_R$

If the assumptions of weak turbulent and orbital rotational effects are satisfied, then the method previously described is capable of building $\tilde{\mathbf{v}}_P$ in the time domain. Coming back to (6), it is then possible to remove $\tilde{\mathbf{v}}_P$ from the total fluctuation $\mathbf{v}$ and to obtain a new velocity signal γ defined as

$$\gamma = \mathbf{v} - \tilde{\mathbf{v}}_P = \mathbf{v}' + \tilde{\mathbf{v}}_R \qquad (22)$$

The problem is now to separate the two remaining contributions $\mathbf{v}'$ and $\tilde{\mathbf{v}}_R$ without knowing any of them. Considering the limitations pertaining to the determination of $\tilde{\omega}$ the only simple way to obtain informations about $\mathbf{v}'$ and $\tilde{\mathbf{v}}_R$ is to take advantage of the correlation property between $\tilde{\mathbf{v}}_R$ and η. For the periodic waves considered in the present section a straightforward separation method could be performed by applying the phase-averaging procedure to γ. In view of a direct extension to random waves we prefer to explore a more general method. The idea is to apply the linear filtration technique (LFT) of *Benilov and Filyushkin* [1970] (see also *Benilov et al.* [1974]) to γ and not to the total signal $\mathbf{v}$ as is usually done.

Let us first recall the guidelines and assumptions of the classical LFT. In this approach the total fluctuating motion is split as

$$\mathbf{v} = \mathbf{v}_o + \mathbf{v}_r \tag{23}$$

where the orbital motion $\mathbf{v}_o$ is defined as the part of $\mathbf{v}$ which is linearly coherent with the surface displacement measured at the same fetch. Under this assumption the power spectrum of any component v_{oi} of $\mathbf{v}_o$ can be computed without reconstructing the realization $v_{oi}(t)$ by the expression

$$S_{v_{oi}v_{oi}} = \frac{S_{v_i\eta}\, S^*_{v_i\eta}}{S_{\eta\eta}} \tag{24}$$

where $S_{v_i\eta}$ is the cospectrum between the wave elevation and the component v_i of the total velocity fluctuation (the star in (24) stands for complex conjugation). Since the remaining contribution $\mathbf{v}_r$ (not to be confused with $\tilde{\mathbf{v}}_R$) satisfies necessarily $\overline{\mathbf{v}_r\eta} = 0$, the assumption of linearity implies

$$S_{v_{oi}v_{ri}} = S_{v_{ri}v_{oi}} = 0 \tag{25}$$

The spectrum of the remaining "turbulent" contribution is thus given by orthogonality as

$$S_{v_{ri}v_{ri}} = S_{v_iv_i} - S_{v_{oi}v_{oi}} \tag{26}$$

It must be kept in mind that since the method is linear, the definition of the orbital motion $\mathbf{v}_o$ resulting from (24) corresponds only to the linear part $\tilde{\mathbf{v}}_{P1}+\tilde{\mathbf{v}}_{R1}$ of $\tilde{\mathbf{v}}$ ($\tilde{\mathbf{v}}_{R1}$ being the rotational counterpart of $\tilde{\mathbf{v}}_{P1}$). All the nonlinear orbital contributions ($\tilde{\mathbf{v}}_{P2}+\tilde{\mathbf{v}}_{R2}$) are thus projected onto $\mathbf{v}_r$.

Let us now apply the same formal method to γ instead of $\mathbf{v}$. Since no assumption of irrotationality is made in the LFT, we get from (22) and (4)

$$S_{\tilde{v}_{R1i}\tilde{v}_{R1i}} = \frac{S_{\gamma_i\eta}\, S^*_{\gamma_i\eta}}{S_{\eta\eta}} \tag{27}$$

Similarly, following (26) the turbulent fluctuation $\mathbf{v}_t$ can be obtained as

$$S_{v_{ti}v_{ti}} = S_{\gamma_i\gamma_i} - S_{\tilde{v}_{R1i}\tilde{v}_{R1i}} \tag{28}$$

Equation (27) makes the extraction of the $\tilde{\mathbf{v}}_{R1}$ spectrum theoretically possible. In the case of a periodic wave train the spectrum of γ is the sum of a continuous spectrum corresponding to the turbulent motion and of discrete rays corresponding to the orbital rotational motion. Equation (27) allows extraction of the energy contained in these rays which is associated with the part of the orbital rotational motion linearly related to η. Naturally, $\tilde{\mathbf{v}}_{R2}$ cannot be obtained from (27). However, it can be shown theoretically [*Magnaudet and Masbernat*, 1990] that $\tilde{\mathbf{v}}_{R1}$ and $\tilde{\mathbf{v}}_{R2}$ are 1 order of magnitude smaller than $\tilde{\mathbf{v}}_{P1}$ and $\tilde{\mathbf{v}}_{P2}$, respectively. Since the part $\tilde{\mathbf{v}}_{P2}$ of $\tilde{\mathbf{v}}_P$ which is nonlinearly related to η is generally itself at least 1 order of magnitude smaller than its linear counterpart, $\tilde{\mathbf{v}}_{P1}$, it can be concluded that the contribution $\tilde{\mathbf{v}}_{R2}$ is at least 2 orders of magnitude smaller than $\tilde{\mathbf{v}}_{P1}$. This means that $\tilde{\mathbf{v}}_{R2}$ is negligible from an energetic point of view and that (27) contains the leading part of the total orbital rotational contribution $\tilde{\mathbf{v}}_R$. Obviously, $\tilde{\mathbf{v}}_{R2}$ is rejected into $\mathbf{v}_t$. Thus this latter quantity is not strictly identical to the turbulent fluctuation $\mathbf{v}'$ defined by (6). However, in practical applications, $\mathbf{v}'$ is at least of the same order of magnitude as $\tilde{\mathbf{v}}_{R1}$. Consequently, $\mathbf{v}_t$ is a good approximation of $\mathbf{v}'$.

The determination of $\tilde{\mathbf{v}}_{R1}$ based on (27) has two shortcomings. The first is that since $\tilde{\mathbf{v}}_{R1}$ is obtained through a filtration technique without any input of physics, there is no proof a priori that the extracted velocity field carries the vorticity of the orbital flow. This must be proved a posteriori, and in the section 2.5, $\tilde{\mathbf{v}}_{R1}$ (which hereafter will no longer be distinguished from $\tilde{\mathbf{v}}_R$) will be shown to bear the desired features. The second limitation of (27) is, of course, that only the power spectrum of $\tilde{\mathbf{v}}_R$ is obtained, whereas the signal $\tilde{\mathbf{v}}_R(t)$, as well as $\tilde{\omega}$, remain unknown. As a consequence, correlations involving $\tilde{\mathbf{v}}_R$ cannot be directly computed. However, since the instantaneous signals $\tilde{\mathbf{v}}_P$ and γ are available, this difficulty can be easily overcome. From (4) and the definition of $\tilde{\mathbf{v}}_{P1}$ as the linear part of $\tilde{\mathbf{v}}_P$, the correlation $\overline{\tilde{v}_{Ri}\tilde{v}_{P1j}}$ can be obtained as

$$\overline{\gamma_i\tilde{v}_{P1j}} = \overline{(\tilde{v}_R + v')_i\tilde{v}_{P1j}} = \overline{\tilde{v}_{Ri}\tilde{v}_{P1j}} \tag{29}$$

2.5. Application to a Rotational Periodic Wave: The Gerstner Wave

From a methodological point of view, the principal difficulty of the present separation method is that the rotational motion, which is a small quantity, is computed as a difference between two large quantities (i.e., the total fluctuating velocity and the potential part of the orbital velocity). Thus before dealing with wind waves, it is of primary importance to prove that the computational precision of all the steps of the method is sufficient for this small quantity to represent a good approximation of the real orbital rotational motion. The simplest conclusive test that can be made consists of checking the method against a theoretical wave solution carrying vorticity.

As reported by *Lamb* [1932, p. 422], an exact rotational solution to the problem of surface waves was given by Gerstner. In this solution, fluid particles describe circular orbits, and their trajectories are given as

$$x = x_0 - ae^{kz_0}\sin(kx_0 - \sigma t) \tag{30a}$$

$$z = z_0 + ae^{kz_0}\cos(kx_0 - \sigma t) \tag{30b}$$

where a is the wave amplitude and (x_0,z_0) denote the mean position of the particle. The Gerstner wave is a finite amplitude wave traveling at the phase speed $c = \sigma/k = (g/k)^{1/2}$. Deriving the equation of the velocity field, it is easy to show that (30a) and (30b) lead to a nonzero horizontal mean current $\overline{U}(z)$ given by

$$\overline{U}(z) = -(ak)^2 c\, e^{2kz_0} \tag{31}$$

This second-order, adverse mean current decays exponentially with depth, has the same magnitude as the

Stokes drift, and thus guarantees a zero net mass transport. The second-order vorticity corresponding to the solution (30a) and (30b) has a magnitude

$$\omega_G = -2\sigma \frac{(ak)^2 e^{2kz_0}}{1-(ak)^2 e^{2kz_0}} \tag{32}$$

Only a part of ω_G correponds to the mean current $\overline{U}(z)$, whereas the remaining is the vorticity of the orbital rotational motion we want to determine.

Our test is carried out on a Gerstner wave corresponding to ak = 0.25 and a = 7.24 mm. The shape of the free surface $\eta(x,t)$, as well as the velocity components u and w at 10 different depths z_i are generated at the fixed fetch x=0. The data set $\eta(0,t)$, $u(0,z_i,t)$ and $w(0,z_i,t)$ is similar to the experimental data that would be obtained by recording the surface displacement at a given fetch and the velocity fluctuations at several depths below the surface at the same fetch. Finally, according to (21), U_l is set to a value compatible with the surface values of the drift current (31) and the vorticity (32). The whole set of data is processed through the complete two-step separation method described in the previous sections.

The first result is that the "turbulent" moments $\overline{u_t^2}$ and $\overline{w_t^2}$ are found negligibly small. This means that the method recognizes, as it has to do, the total velocity fluctuations u and w as being correlated to the surface displacement η. As discussed before, the accuracy of the determination of $\tilde{\mathrm{v}}_R$ has to be proved indirectly since the method is unable to build $\tilde{\omega}$. For that purpose, let us consider the general identity which holds for a two-dimensional flow

$$\frac{\partial}{\partial z}(u^2 - w^2) = 2u\omega + 2\frac{\partial}{\partial x}(uw) \tag{33}$$

For a periodic motion the last term vanishes. Using the fact that $\overline{\tilde{u}_P^2} = \overline{\tilde{w}_P^2}$, (33) applied to the fluctuating motion writes

$$\frac{\partial}{\partial z}\left[\overline{\tilde{u}_R^2} - \overline{\tilde{w}_R^2} + 2(\overline{\tilde{u}_P\tilde{u}_R} - \overline{\tilde{w}_P\tilde{w}_R})\right] = 2\overline{\tilde{u}\tilde{\omega}} \tag{34}$$

Equation (34) provides the basis of the test; $\overline{\tilde{u}_R^2}$ and $\overline{\tilde{w}_R^2}$ are directly computed through (27), while $\overline{\tilde{u}_P\tilde{u}_R}$ and $\overline{\tilde{w}_P\tilde{w}_R}$ arise from (29). The result is then differentiated with respect to z and compared to the quantity $2\overline{\tilde{u}\tilde{\omega}}$ provided by the theoretical solution. This comparison is illustrated in Figure 1. It can be seen that the left-hand side of (34) given by the separation method agrees very well with the theoretical solution over the whole depth. This proves that provided the physical assumptions made in subsection 2.2 are satisfied, the present method is sufficiently accurate to give relevant information about the orbital rotational motion, even if this contribution is only a small part of the total motion. Furthermore, this test allows to verify that the method only requires an accurate description of the mean motion in the surface region; in the present case a linear shear flow was used to model an exponential current without any damage for the determination of both potential and rotational orbital motions.

3. Extension of the Method to Laboratory Wind-Generated Waves

3.1. General Considerations

Having shown that the separation method gives reliable results for periodic two-dimensional waves, we turn now to our central objective, i.e., its generalization and its application to laboratory, wind-generated waves. In this context, the definition (1)-(3) of the orbital motion obtained for periodic waves through the concept of phase averaging is no more applicable. This definition can be made more general by considering the orbital motion as the part of v which is related to the displacement η of the free surface, whatever its state of coherence. This relation whose exact expression is generally unknown can be written under the functional form

$$\tilde{\mathrm{v}}(x,y,z,t) = F[\eta(x_s,y_s,\tau)], \quad z(x_s,y_s) \in S_{urf}, \tau \in \,]-\infty, t] \tag{35}$$

where S_{urf} denotes the free surface. In contrast no such relation is supposed to exist between v' and η, so that (4) is assumed to remain valid. Having defined the orbital velocity by (35),

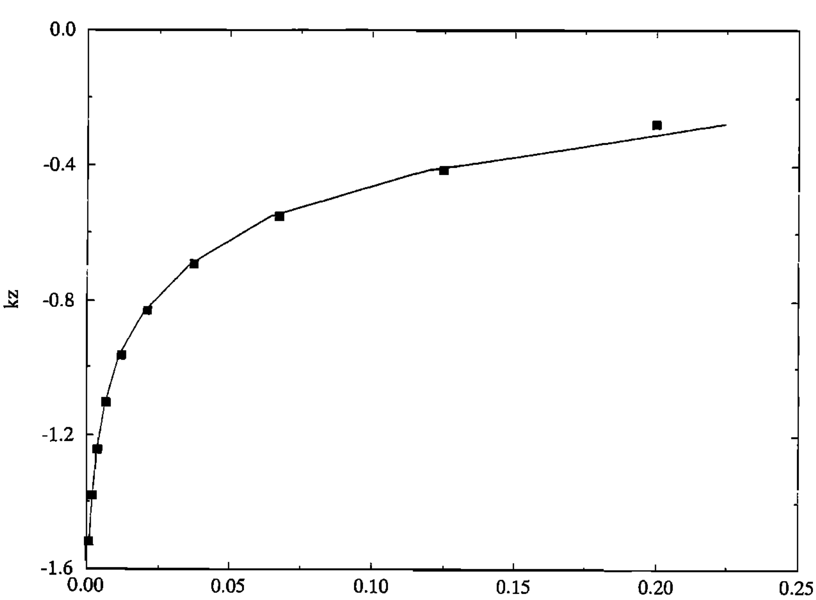

Figure 1. Correlations involving the orbital vorticity below a Gerstner wave. Squares are $\partial/\partial z(\overline{\tilde{u}_R^2} - \overline{\tilde{w}_R^2} + 2(\overline{\tilde{u}_P\tilde{u}_R} - \overline{\tilde{w}_P\tilde{w}_R}))$; curve is $2\overline{\tilde{\omega}\tilde{u}}$; normalizing parameter is $1/2a^2k^3c^2$.

the Helmholtz decomposition (5) can be performed on $\tilde{\mathbf{v}}$ and the triple decomposition (6) can be applied to the total fluctuating velocity **v**.

A first extension of the Dean method to a wind-generated wave field was made by *Jiang et al.* [1990]. These authors assumed that the whole orbital motion could be described by a stream function of the form

$$\Psi_p(x',z)=\sum_{n=1}^{N}\exp(n\Delta kz)\,(X_{2n-1}\cos n\Delta kx'+X_{2n}\sin n\Delta kx') \quad (36)$$

This stream function has the same form as that defined in (18), with k_0 replaced by Δk. However, its meaning is very different; while (18) describes the motion of a carrier wave (with wave number k_0) and its harmonics, (36) is intended to build a discrete approximation of a continuous spectrum with a spatial resolution Δk. *Jiang et al.* [1990] applied (36) to laboratory data and used the results to investigate wave-turbulence interactions. In their work several key hypotheses are made, namely that the orbital motion is (1) potential and (2) two-dimensional, and (3) that all components of the wave spectrum move at the same phase velocity c as the dominant wave. Furthermore, the orbital motion is assumed not to be affected (4) either by the mean shear current (5) or by the turbulence.

As previously discussed, assumptions (1) and (4) are not retained in the present work. Assumption (1) implies that the orbital rotational motion is rejected into the "turbulent" contribution, and this is clearly in conflict with the triple decomposition in (6). Assumption (4) seems hardly tenable since the wind-induced shear current greatly affects the propagation of laboratory wind waves, as pointed out in subsection 2.3. Disregarding both these assumptions, a very straightforward way to extend our separation method to laboratory wind waves would be to use the stream function (36) in place of (18) to determine $\tilde{\mathbf{v}}_P$. However, this approach is acceptable only if the remaining assumptions are proved to be valid. Thus we begin by examining both assumptions (2) and (3). Assumption (5) which is needed to obtain separate governing equations for the orbital potential motion, as in the case of periodic waves, will be checked a posteriori.

To discuss these assumptions and describe the final method, we use wind wave data coming from experiments undertaken in the Institut de Mécanique des Fluides de Toulouse (IMFT) wind-water tunnel facility. The characteristics of the facility, as well as the experimental procedure, are thoroughly described in the companion paper MT. Measurements have been performed at a fetch of 13 m for four wind regimes as follows: 4.5, 6.8, 9.0, and 13.5 m/s. Water velocity measurements have been carried out with a submersible laser optical fiber system, making possible measurements of the spanwise component, while free surface elevation and phase velocities have been determined using two capacitance gauges aligned with the wind direction.

3.2. On the Three-Dimensionality of the Wave Field

The question of whether or not laboratory wind waves can be satisfactorily regarded as two-dimensional is not easy to answer. At sea it is quite well established that conjugate effects of variations of the wind conditions and three-dimensional wave instabilities produce a pronounced directional structure of wind wave spectra. *Yefimov et al.* [1972] established that this structure is fairly well described by a $\cos^2\Theta$ dependence of the directional energy spectrum (Θ denoting the angle between the wind direction and the local direction). The situation is quite different in laboratory studies. The main specificity of laboratory experiments is that wind always blows along the same direction and that the lateral walls play the role of a waveguide. Clearly, the phases of all components of the wave field are forced to satisfy a relation ensuring that spanwise motions vanish on the sidewalls. Thereby, compared with field situations, the development of spanwise motions is reduced, especially when the width of the channel is comparable to the dominant wavelength [*Longuet-Higgins*, 1990].

The best illustration of the weakness of spanwise motions associated with the waves is probably provided by a comparison of the intensities of the spanwise and streamwise (or vertical) fluctuating motions. Figure 2 depicts such a comparison performed with the data obtained in our facility at a wind speed of 9.0 m/s. It is clear that in the entire region influenced by the waves the spanwise fluctuation v is smaller than the vertical fluctuation w. The typical exponential decay of the orbital potential velocity associated with the dominant wave is also shown in Figure 2. This decay is very similar to that found on the w profile, whereas the v profile exhibits a completely different and much more rapid decay. This is a clear indication that there is no noticeable orbital component in the spanwise direction or more precisely that the orbital motion dominates w (except at large distances from the surface), whereas the turbulent contribution dominates v.

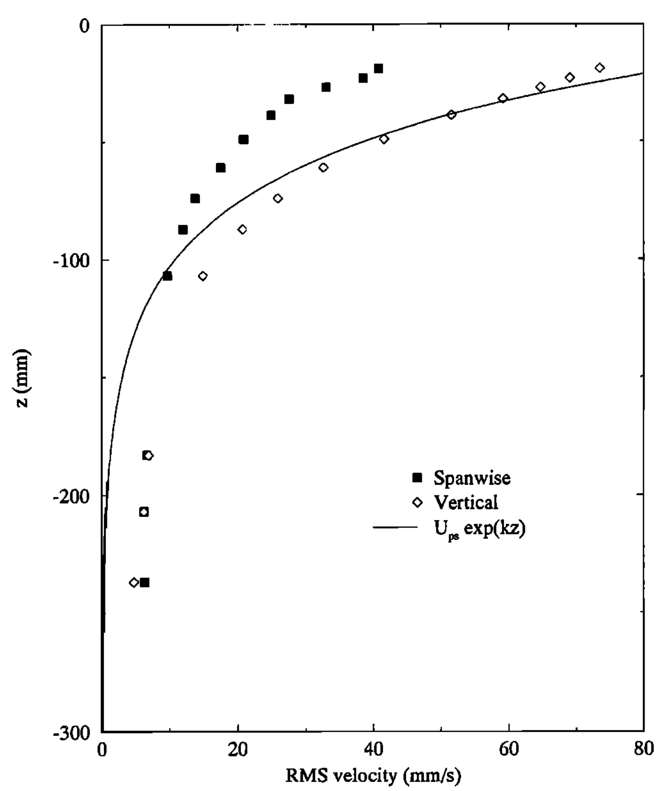

Figure 2. Vertical and spanwise total rms velocities; Wind speed U_∞=9.0 m/s, solid squares indicate spanwise velocity; open diamonds, vertical velocity; curve is U_{ps} exp(kz), with U_{ps} defined as the surface orbital velocity estimated from wave spectrum.

3.3. The Question of Dispersion

In their extension of the *Dean* [1965] method to wind waves, *Jiang et al.* [1990] assumed that all wave components propagate at the phase velocity c of the dominant wave. This hypothesis seems physically dubious since it goes against the well-known dispersive behavior of gravity waves. However, it can be appropriate for studying laboratory wind waves because of two specificities. The first one is the nondispersive behavior of young wind waves reported by *Ramamonjiarisoa* [1974] and *Coantic et al.* [1981] and justified theoretically by *Lake and Yuen* [1978]. These studies show that owing to nonlinear interactions, the wave field can be dominated by components behaving as bounded harmonics of the dominant wave. The assumption of a unique phase velocity for this part of the wave field is thus fully justified. Recent laboratory studies using bispectral analysis [*Leykin et al.*, 1993] confirm that such wave components carry a significant part of the wave energy, while the other part lies in free waves. The problem of dispersion occurs for this second part of the spectrum consisting in free waves. This is where the second specificity of laboratory wind waves occurs. It lies in the very sharp form of the spectra; even for waves obeying the usual dispersion relation, dispersion with respect to the dominant wave becomes appreciable only for components lying far from it. Since for a sharp spectrum the energy associated with such components is weak, dispersive effects can become indiscernible in (15)-(16).

Such an influence of the shape of the spectra on dispersive effects can be checked following a simple way. The first step is to build numerically a collection of small-amplitude waves with random phases in uniform deviates, i.e.,

$$\eta(x,t) = \int A(k)\cos[k.x - \sigma(k)t + \theta(k)]\,dk \qquad (37)$$

where $A(k)$ is the amplitude wave number spectrum. The surface elevation $\eta(x,t)$ is made up of multicomponent linear waves, each of them traveling with its own phase speed as given by the linear dispersion relation. The generation of such a wave train involves two leading parameters; one is the local energy maximum S_i of the ith component centered on wave number k_i, while the other is the relative width of each peak denoted as $W_i = \Delta k_i / k_i$. Note that such spectra are not intended to represent real wave spectra but only to allow a quantitative study of dispersive effects on (15)-(16) for a given spectral distribution and a perfectly known dispersion relation. Since $A(k)$ and $\theta(k)$ are arbitrary, (37) cannot represent a nonlinear wave field and only linear tests can be performed using this distribution. Figure 3 shows two frequency spectra normalized by S_0; both of them correspond to $\Delta k_i / k_i = 0.2$. The two spectra only differ by the relative amplitude of higher harmonics which obeys $S_i = S_0/(i+1)$ for spectrum S_1 and $S_i = S_0/(i+1)^2$ for spectrum S_2 ($i \in [0,5]$). The second step of the test consists of solving the linear counterpart of (15)-(16) ((B2)-(B3) in appendix B), with the aid of the stream function (36) (no mean current assumed). Figure 4a shows that the results obtained with spectrum S_1 are very bad; the method is unable to reproduce either the given surface elevation or to satisfy the Bernoulli equation with a constant right-hand side. This proves simply that if the waves are dispersive and if the energy located far from the dominant wave is significant, then the system (15)-(16) and (36) has no solution. This illustrates the exact signification of the dispersion relation which expresses a compatibility condition for (15) and (16) to be both verified on the same given surface. Figure 4b depicts the results of the same test performed on spectrum S_2. The results are much more satisfactory, even if the right-hand side of the Bernoulli equation still varies slightly. The results confirm that with such a spectral distribution, dispersive effects are too weak to affect significantly (B2) and (B3) in appendix B.

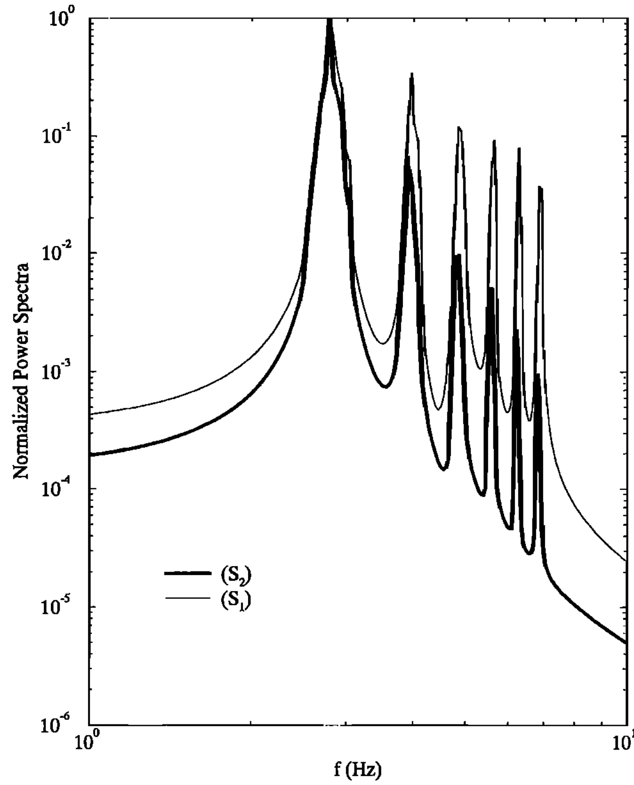

Figure 3. Frequency power spectra of numerically generated dispersive random wave fields. Local maxima behave as $S_1, S_i = S_0/(i+1)$ (thin solid curve) and S_2, $S_i = S_0/(i+1)^2$ (thick solid curve).

Real wind wave spectra obtained in laboratory experiments are generally sharper than the fictitious spectrum S_2. Considering the results of the foregoing test and the nondispersive behavior of a significant part of the wave field, it seems reasonable to assume that for such waves the problem (15)-(16) can be adequately resolved by neglecting dispersion. Consequently, we apply the stream functions (19) and (36) to solve the problem (15)-(16) for a real wave record. Figure 5 confirms for a typical block of real data, including nearly 20 periods of the dominant wave, that measured and predicted wave elevations $\eta_m(t)$ and $\eta_p(t)$ are in very good agreement while the right-hand side Q of Bernoulli equation remains almost constant. Only small-amplitude displacements associated with high frequencies are not very accurately followed because they do not contribute much to the error to be minimized and the number of Fourier modes kept is not sufficient to describe them properly. This typical result demonstrates that owing to the physical characteristics of laboratory wind waves, the form (36) of Ψ_P which assumes that all components of the wave spectrum travel at the same phase velocity enables us to satisfy with good accuracy both (15) and (16).

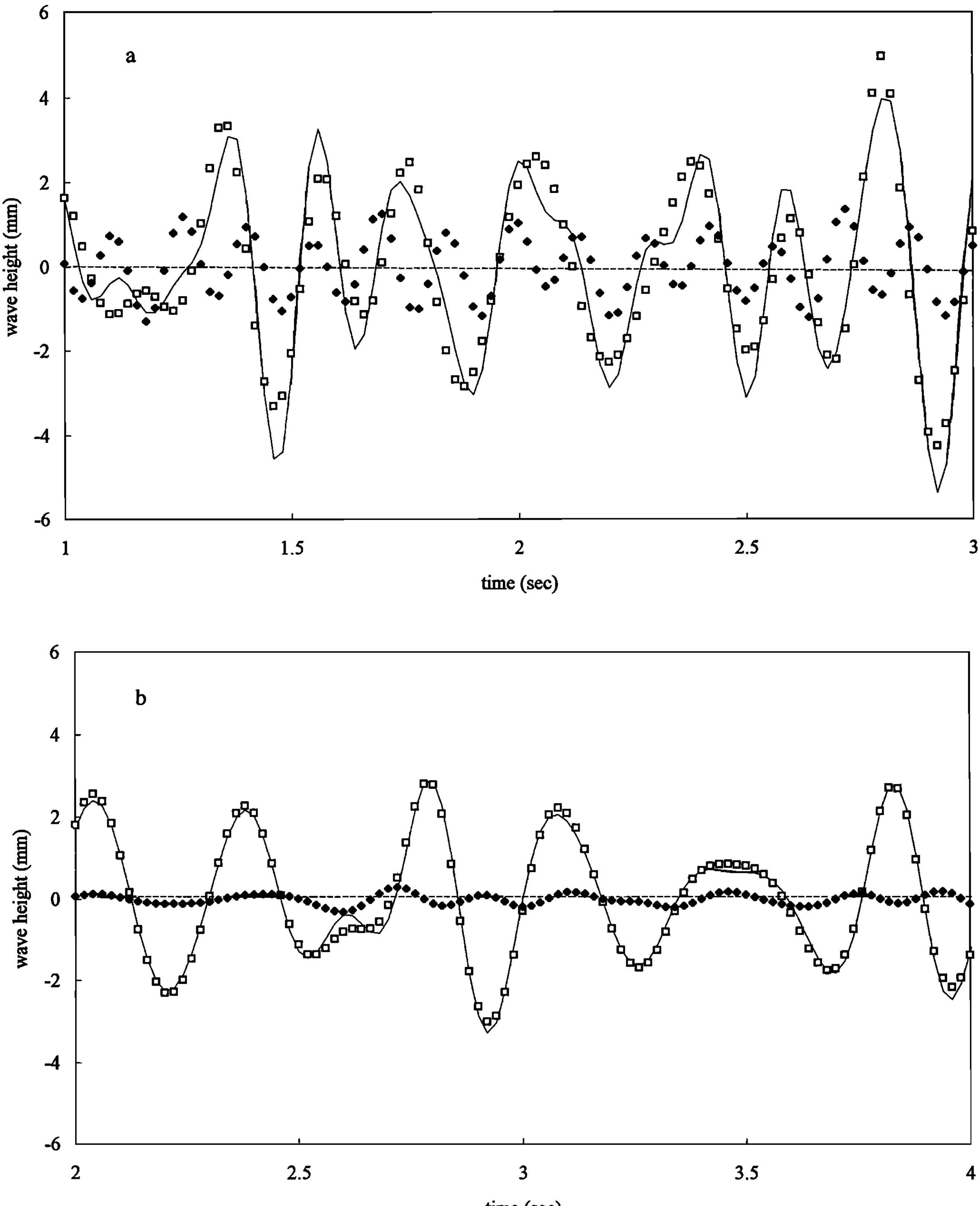

Figure 4. Result of linear separation method applied to numerically generated dispersive random wave fields. Local maxima behave as (a) $S_i=S_0/(i+1)$ and (b) $S_i=S_0/(i+1)^2$. Solid curve is wave data η_m; open squares, computed wave η_p; and solid diamonds, $Q_k-\overline{Q}$.

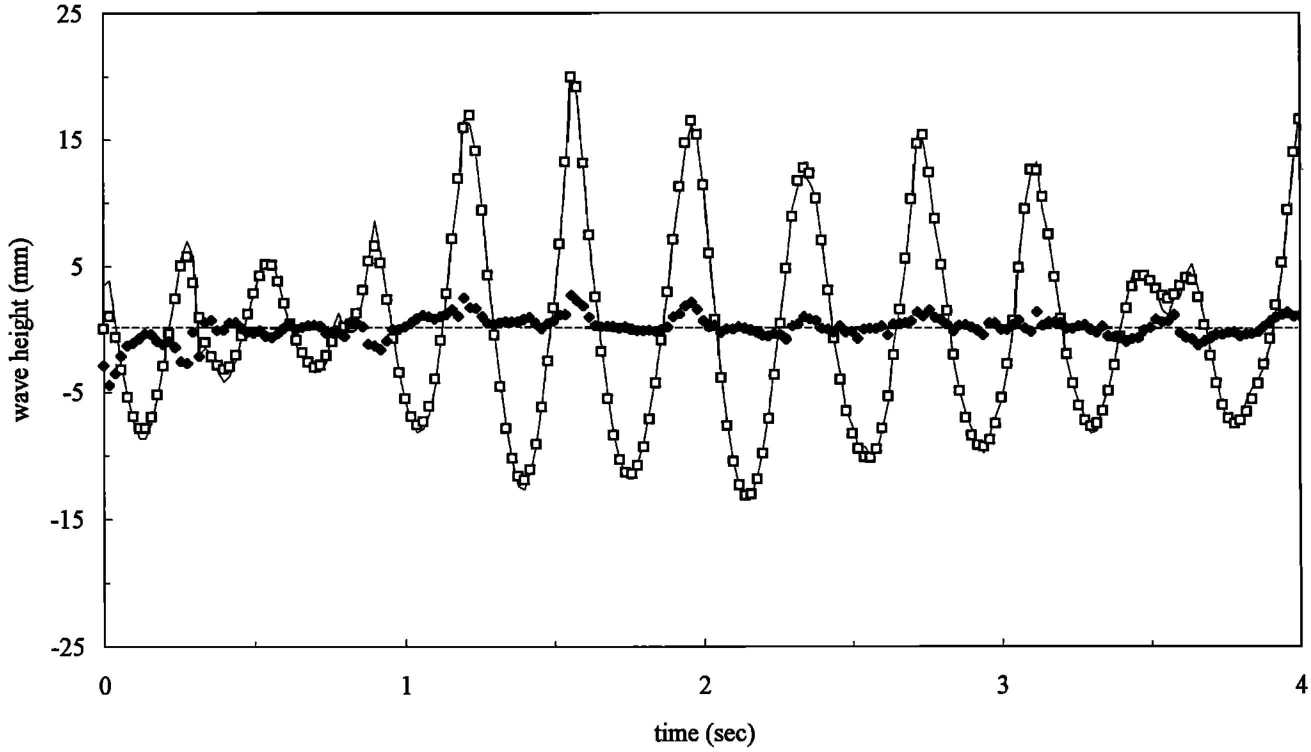

Figure 5. Sketch of laboratory wind waves (Wind speed U_∞=9.0 m/s) and result of nonlinear triple decomposition method (TDM). Solid curve is wave data η_m; open squares, computed wave η_p; and solid diamonds, $Q_k - \overline{Q}$.

3.4. The Triple Decomposition Method

The foregoing conclusions concerning the weakness of the spanwise orbital motions and the lack of significant effects of dispersion on (15)-(16) for laboratory wind wave data suggest a reasonable generalization to wind waves of the method developed in section 2. Having measured the wave elevation $\eta(x_0,t)$ at a fetch x_0 and determined the phase velocity of the dominant wave $c(k_0)$ and the Lagrangian drift current U_l, the orbital potential motion is first obtained by solving (15)-(16) with $\overline{\Psi}$ and Ψ_p given by (19) and (36), respectively. The lagrangian drift U_l is related to U_0 and U_0' through (A9) which generalizes (21) to random waves. Then, as in the case of periodic waves, the orbital potential motion $\tilde{\mathbf{v}}_P$ derived from (36) is substracted from the total measured fluctuation **v**. Finally, the spectra of $\tilde{\mathbf{v}}_R$ and **v'** are obtained by applying (27) and (28) to the signal **v**-$\tilde{\mathbf{v}}_P$ as described in subsection 2.4. Details about the implementation of the general method used to determine $\tilde{\mathbf{v}}_P$, its linear version (used to obtain $\tilde{\mathbf{v}}_{P1}$), and the choice of the parameters can be found in appendix B. An important question concerns the final precision of the method. An indication about this point is provided by the residual kinetic energy K_{Res} associated with the error E_T made in the minimization procedure (see (B1)). K_{Res} defined as $K_{\mathrm{Res}} = 1/2(c_0/c)^2\omega_0{}^2E_T$ is shown at the end of Table 1. Table 1 also summarizes the values of kinetic energies K_{P1}, K_R, K_C, and K_T associated with the linear part of the orbital potential and rotational motions, mean current, and turbulent motion, respectively, all taken at the closest point below the waves. These results suggest that K_{P1}, K_C, and K_T are determined with a very good accuracy. Concerning the orbital rotational motion, the ratio K_{Res}/K_R lies roughly between 8% and 16%, suggesting that the orbital rotational motion is determined with a precision of nearly 20%. This indicates that the order of magnitude of the momentum fluxes associated with the orbital rotational motion can be obtained through the present method, even if a significant uncertainty exists on the precise value of these terms.

3.5. Turbulent and Rotational Contributions Near the Surface

Turning back to the assumptions listed in subsection 3.1, as well as to those made to simplify (12) for obtaining (16), it appears that the method is valid only if rotational and turbulent effects are sufficiently weak on the surface. We are

Table 1. Kinetic Energies of the Different Motions at the First Measured Point Below the Surface

U_∞ m/s	K_T cm²/s²	K_R cm²/s²	K_{P1} cm²/s²	K_{P2} cm²/s²	K_C cm²/s²	K_{Res} cm²/s²
4.5	3.0	1.0	14.4	0.04	23.7	0.14
6.8	5.9	0.9	26.5	0.08	24.4	0.15
9.0	6.3	1.6	34.0	0.09	16.0	0.14
13.5	12.5	2.6	60.5	0.32	23.9	0.23

Abbreviations are U_∞, wind speed; K_T, K_R, K_{P1}, K_{P2}, and K_C are the kinetic energies associated with the turbulent motion, the rotational orbital motion, the linear part of the potential orbital motion, the nonlinear part of the potential orbital motion, and the mean current, respectively. K_{Res} is the residual kinetic energy associated with the final error made in the minimization procedure (see subsection 3.4).

unable to check precisely this hypothesis since the distribution of $\overline{\tilde{v}_{Ri}^2}$ and $\overline{v_i'^2}$ right on the surface is unknown. However, we can try to estimate qualitatively the effect of the neglected terms by looking at the values of the kinetic energies shown in Table 1. K_{P1} and K_C appear clearly as the major terms. This result proves that it is absolutely necessary to take the mean current into account and that it is correct, at leading order, to neglect rotational and turbulent effects in the determination of the linear part $\tilde{v}_{P1}$ of $\tilde{v}_P$. Since correlations like $\overline{\tilde{v}_{Ri}^2}$ and $\overline{\tilde{v}_{P1i}\tilde{v}_{Rj}}$ are determined by removing $\tilde{v}_{P1}$ from the measured fluctuation and then applying LFT, it can be concluded that the process used to evaluate these correlations is coherent with the order of magnitude analysis. In contrast, the kinetic energy K_{P2} associated with the nonlinear part of the orbital potential motion is found to be smaller than K_T or K_R and even K_{Re_s}. Hence it is probably incorrect to determine $\tilde{v}_{P2}$ without taking into account the effects of $\tilde{v}_R$ and v'. This means that owing to the poor determination of $\tilde{v}_{P2}$, a small error certainly exists in the turbulent fields determined by the method.

3.6. The Effect of the Mean Sheared Current on $\tilde{v}_P$

As is well known from wave theory, the amplitude of $\tilde{v}_P$ is directly proportional to the relative phase speed c_0. Since in the present method $\tilde{v}_P$ must be removed from v to obtain $\tilde{v}_R$, it is of primary importance that c_0 be accurately evaluated. In fact, both relative and absolute phase velocities are needed to determine $\tilde{v}$; definition of the moving fetch $x' = x - ct$ clearly involves the absolute phase velocity determined experimentally. In contrast, the relative phase velocity c_0 appears in the definition of the mean current (see (20)). In this subsection we stress that the determination of $\tilde{v}_P$ can be dramatically affected by the value of c_0 used in (20). The simplest way to determine c_0 would be to assume U_0=0, so that $c = c_0$. However, laboratory data do not support such simplification; for example, in present data the ratio U_l/c ranges from 20% at U_∞=4.5 m/s to 40% at U_∞=13.5 m/s. This fact was also pointed out by *Jiang et al.* [1990], who found absolute phase speeds up to 30% higher than those given by the linear dispersive law. A sounder estimate of c_0 valid for a linear mean current is given in appendix A in terms of c, U_l, and U_0'. From (A11) it can be written:

$$c_{0e_1} = c\,\{1+\varepsilon^2\delta - U_l/c + [(1+\varepsilon^2\delta - U_l/c)^2 + 2(1-\varepsilon^2)\varepsilon^2\delta^2]^{1/2}\}/[2(1-\varepsilon^2)] \tag{38}$$

where ε is a measure of the wave slope ($\varepsilon^2 = 2\overline{\eta^2}(\omega_0/c)^2$) and δ stands for U_0'/ω_0, ω_0 being the radian frequency $2\pi f_0$. Usually, U_0' is not determined directly in the measurements. Since $\varepsilon\delta$ can be verified to be small compared to unity, a simpler estimate involving only basic experimental data is given by

$$c_{0e_2} = \frac{c - U_l}{1 - \varepsilon^2} \tag{39}$$

Equation (38) or (39) could be used directly in the separation method and should provide good estimates of c_0. In fact, we prefer to start from (A9) which is slightly more general. Comparisons of the phase speed c_0 determined numerically by the triple-decomposition method with the estimate (38) show a very close agreement. The value provided by (39) is still in fairly good agreement, even if the difference increases with U_∞ as a consequence of the neglect of U_0'.

Interestingly, the value of c_0 provided by the method can also be compared with those given by various forms of the dispersion relation. The linear dispersion relation arising from (15) and (16) satisfies

$$c_0^2\left(1+\frac{U_0'}{\omega_0}\right)+\frac{c_0}{\omega_0}\left(U_0'U_0-g\right)-\frac{gU_0}{\omega_0}=0 \tag{40}$$

With the aid of (A8) this leads to a value c_{0d_1} of c_0 given by a cubic equation. If U_0' is not taken into account, the solution of (40) reduces to

$$c_{0d_2} = \frac{g(1-\varepsilon^2)}{2\omega_0} + \left[\left(\frac{g(1-\varepsilon^2)}{2\omega_0}\right)^2 + \frac{gU_l}{\omega_0}\right]^{1/2} \tag{41}$$

Finally, if U_0 is also neglected, the well-known dispersion relation is recovered

$$c_{0d_3} = \frac{g}{\omega_0} \tag{42}$$

Figure 6 compares the value of c_0 given by the TDM (hereafter denoted $c_{0\mathrm{TDM}}$) to the absolute phase velocity c and to values c_{0d_1}, c_{0d_2}, c_{0d_3} predicted by the various forms of the dispersion relation (values predicted by (40) are not shown since they are very close to the TDM prediction, whatever U_∞). Obviously, $c_{0\mathrm{TDM}}$ lies below c at all winds. Antagonistic effects of the mean sheared current can be observed by comparing the evolution of $c_{0\mathrm{TDM}}$ with that of c_{0d_3}. At low winds, c_{0d_3} underpredicts c_0 because the current behaves mainly as a constant drift. In contrast, at high winds, c_{0d_3} overpredicts c_0 because U_0' is large (δ becomes of order unity) and the global effect of the sheared current is then to reduce c_0. Differences between c_{0d_3} and $c_{0\mathrm{TDM}}$ can reach nearly 15%, whereas c_{0d_2} (which takes into account U_0 but neglects U_0') may overestimate c_0 by nearly 50%! This comparison shows that forms (41) and (42) of the dispersion relation are not appropriate for determining c_0 in laboratory wind wave experiments. When these different estimates of c_0 are used to predict $\tilde{v}_P$, the results are very different as shown on a vertical profile in Figure 7; in this example, the amplitude of $\tilde{u}_{P1}$ would be artificially increased by more than 45% if c or c_{0d_2} were used in place of the value of c_0 determined by the TDM. This demonstrates that a necessary condition for predicting accurately $\tilde{v}_P$ is that U_0 and U_0' are both taken into account in the determination of c_0.

3.7. An Example of Results

We present here a typical example of the results given by the whole separation method. For this purpose, we consider velocity measurements of the component w corresponding to the wind speed U_∞=9 m/s. Figure 8 presents the spectra of both the orbital potential and rotational contributions, as well as the turbulent movement. These typical results show that the shape of $S\tilde{w}_R\tilde{w}_R$ follows roughly that of $S\tilde{w}_P\tilde{w}_P$: $S\tilde{w}_R\tilde{w}_R$ reaches its maximum at f=f_0, follows the same slope as $S\tilde{w}_P\tilde{w}_P$ on both sides of f_0 and all the significant components of $\tilde{w}_R$ are

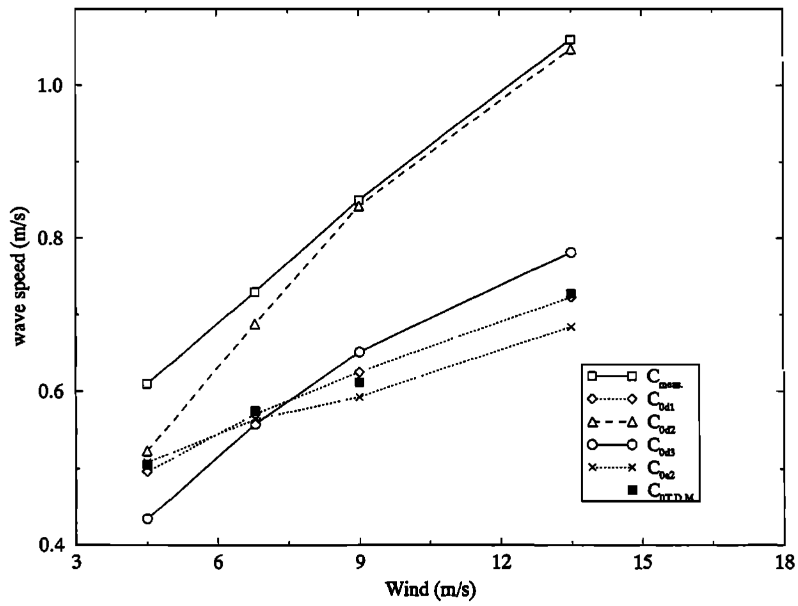

Figure 6. Experimental and theoretical determinations of relative phase velocity c_0. Open squares are c_{mes}; open diamonds c_{0d1}; open triangles c_{0d2}; open circles c_{0d3}; crosses c_{0e2}; and solid squares, c_{0TDM}.

located within a narrow band of frequencies centered on f_0. Theoretical reasons for this similarity are presented in the companion paper MT. It can be noted that the turbulent spectrum exhibits a bump around the dominant wave frequency f_0. This bump whose origin is discussed in MT is present in all turbulent spectra and is much more pronounced on the spectra of the streamwise component u'.

In the present framework the most important feature shown by Figure 8 is the relative magnitude of the orbital rotational motion; $\overline{\tilde{w}_R^2}/\overline{\tilde{w}_P^2}$ is about 5%, whereas the ratio $\overline{\tilde{w}_R^2}/\overline{w'^2}$ reaches 25%. This enforces the idea that owing to the large amount of energy contained in the wave motion, a small deviation from irrotationality can lead to a perturbation of the same order as the turbulent contribution. It is then easy to guess that the orbital rotational motion can play a crucial role in energy transfers between the mean current, the orbital motion, and the turbulent fluctuations.

4. Conclusions

Our main purpose in this work has been to devise a two-step technique for extracting from experimental velocity data the orbital potential and rotational contributions below laboratory wind waves. The problem has been first formulated for two-dimensional periodic waves. The first step of the method consists of a nonlinear formulation allowing the determination of the stream function of the orbital potential motion $\tilde{\mathbf{v}}_P$ when a linear sheared current exists. In a second

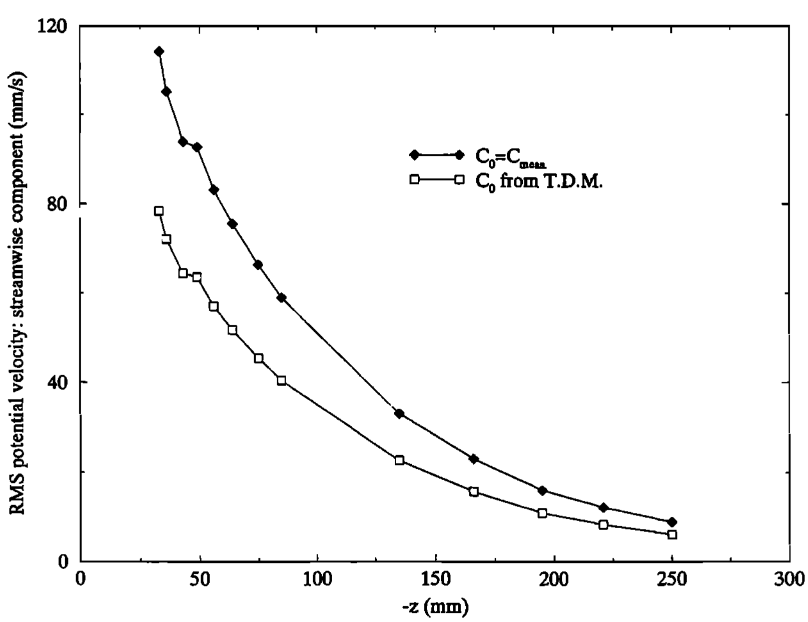

Figure 7. Illustration of the effect of the mean sheared current on the determination of $\tilde{u}_P$. Wind speed U_∞=13.5 m/s. Curves with solid diamonds denote $\tilde{u}_P$ computed with c_{mes}; open squares, $\tilde{u}_P$ computed with c_{0TDM}.

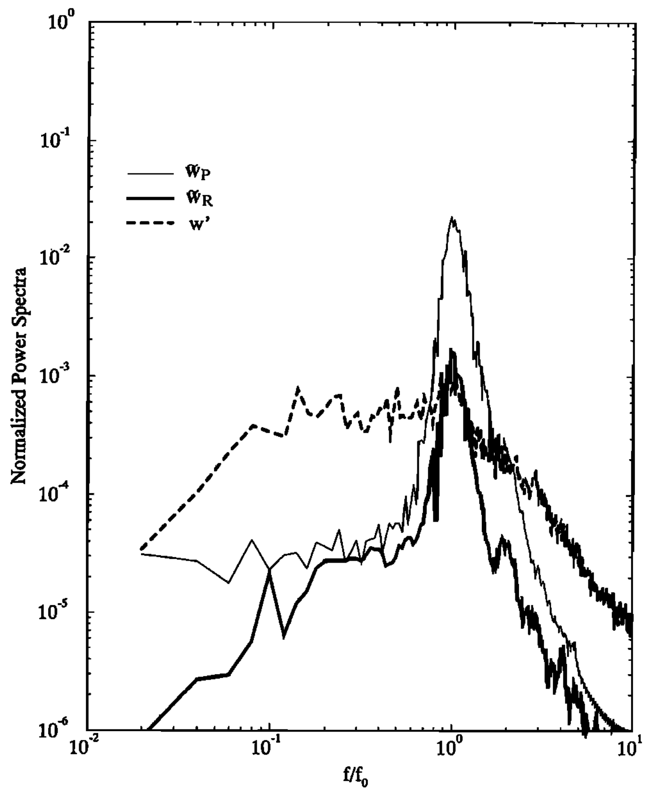

Figure 8. Typical spectra of the three contributions to the vertical velocity fluctuation. Wind speed U_∞=9.0m/s, z = -19 mm. Solid, thin curve is orbital potential velocity; solid, thick curve, orbital rotational velocity; and dashed curve, turbulent velocity.

step the spectrum of the orbital rotational contribution $\tilde{v}_R$ is obtained by means of the linear filtration technique of *Benilov and Filyushkin* [1970] applied to the signal v-$\tilde{v}_R$. That the method is capable of extracting accurately the contribution of the orbital rotational motion has been proved by performing a detailed test on the rotational Gerstner solution. Extension to laboratory wind waves has been made after a discussion of two key points, namely the weakness of both spanwise orbital motions and dispersive effects. Finally, the crucial role played by the mean sheared current in the determination of $\tilde{v}_P$ has been discussed in some detail. We stress the fact that conclusions concerning three-dimensional and dispersive effects apply a priori only to laboratory data and that the method needs certainly improvements before being applicable to the field. However, even with this strong limitation this method is a useful tool for studying interaction mechanisms between wind waves, mean current, and turbulence.

Appendix A: Trajectory of a Water Particle on the Free Surface in Presence of a Mean Linear Current

A1. Periodic Surface Waves

Let us consider on the free surface a water particle whose position was x_0, z=0 at time t=0. The position of this particle at any time t will be

$$x(t) = x_0 + \int_0^t U\{x(\tau),\eta[x(\tau),\tau],\tau\}\,d\tau \qquad \text{(A1)}$$

where the horizontal velocity component can be written as

$$U\{x(\tau),\eta[x(\tau),\tau],\tau\} = U_0 + \eta[x(\tau),\tau]U_0' + \tilde{u}\{x(\tau),\eta[x(\tau),\tau],\tau\} \qquad \text{(A2)}$$

If the current U_0 exists, the trajectories are open since to first order $x(t) - x_0 = U_0 t$. In order to manage a higher-order Taylor expansion of (A1) around a fixed point it is more convenient to work in a frame R'' moving at the constant velocity U_0. In this frame one gets

$$x''(t) - x_0'' = \int_0^t \left(\eta[x''(\tau),\tau]U_0' + \tilde{u}\{x''(\tau),\eta[x''(\tau),\tau],\tau\}\right)d\tau \qquad \text{(A3)}$$

The current being a linear function of depth, the potential linear Airy solution still holds. Thus for a sine wave, η and $\tilde{u}$ are given at first order in the wave slope by

$$\eta(x'',t) = a\cos(kx'' - \omega'' t) \qquad \text{(A4a)}$$

$$\tilde{u}(x'',z,t) = akc_0 e^{kz}\cos(kx'' - \omega'' t) \qquad \text{(A4b)}$$

where $\omega'' = \omega\text{-}kU_0 = k\,(c\text{-}U_0) = kc_0$ is the radian frequency seen in R''. Expansion of (A3) up to second order in the wave slope ak is

$$\begin{aligned} x''(t) - x_0'' = &\int_0^t \left[U_0'\eta(x_0'',\tau) + \tilde{u}(x_0'',0,\tau)\right]d\tau \\ &+ \int_0^t \left[x''(\tau) - x_0''\right]\left[U_0'\nabla_{x''}\eta + \nabla_{x''}\tilde{u}(x_0'',0,\tau)\right]d\tau \\ &+ \int_0^t \eta(x_0'',\tau)\nabla_z\tilde{u}(x_0'',0,\tau)\,d\tau \end{aligned} \qquad \text{(A5)}$$

Averaging (A5) on the wave period T and dividing by T yields the expression of the drift velocity U_s in R''

$$U_s = a^2/2\,c_0(U_0' + kc_0)^2 + 1/2\,a^2k^2c_0 \qquad \text{(A6)}$$

Coming back to the fixed reference frame, the total drift velocity may be written as

$$U_l = U_0 + a^2k^2c_0 + a^2/2U_0'(2k + U_0'/c_0) \qquad \text{(A7)}$$

The second term in the right-hand side of (A7) is the well-known Stokes drift [*Phillips*, 1977, p. 44]. The third term is an additional mass transport contribution which comes from the fact that a particle following the surface sees a mean current different from U_0 because, as shown by *Longuet-Higgins* [1986], the Lagrangian average of $z = \eta(x,t)$ is nonzero.

A2. Extrapolation to Random Waves

As far as the free surface can be regarded as a linear superposition of many sinusoids, the expression of the Lagrangian surface drift U_l can be deduced from (A6) and (A7) as

$$\begin{aligned} U_l = U_0 &+ 2\int(2\pi f)^2\frac{c_0}{c^2}S_{\eta\eta}(f)df \\ &+ U_0'\int\frac{4\pi f}{c}S_{\eta\eta}(f)df + \frac{U_0'^2}{c_0}\int S_{\eta\eta}(f)df \end{aligned} \qquad \text{(A8)}$$

where $S_{\eta\eta}(f)$ denotes the wave power spectrum. If U_l, c and wave-related quantities are known experimentally, (A8) can be used as a relation between U_0 (or c_0) and U_0'. In the framework of the TDM, consistent with the assumption of a non-dispersive wave field, c_0 and c are independent of f, so that (A8) becomes

$$\frac{U_0'^2}{c_0}\int S_{\eta\eta}(f)df+\frac{4\pi U_0'}{c}\int fS_{\eta\eta}(f)df + c_0\left(\frac{8\pi^2}{c^2}\int f^2 S_{\eta\eta}(f)df-1\right)+c-U_l=0 \tag{A9}$$

In the case of a narrowband spectrum centered around frequency f_0, $S_{\eta\eta}(f)$ can be approximated as

$$S_{\eta\eta}(f)=\overline{\eta^2}\ \delta(f-f_0) \tag{A10}$$

Introducing the radian frequency $\omega_0 = 2\pi f_0$, (A9) can then be rewritten as

$$\frac{\overline{\eta^2}}{c_0}\ U_0'^2+\frac{2\omega_0}{c}\ \overline{\eta^2}\ U_0' +\left[2\overline{\eta^2}(\frac{\omega_0}{c})^2-1\right]c_0+c-U_l=0 \tag{A11}$$

Appendix B: Implementation of the Triple Decomposition Method

Only essential guidelines or parameters used in the first step of the method, i.e., the determination of $\tilde{v}_P$, are given here since the original method is extensively described in the paper of *Jiang et al.* [1990]. Schematically, the determination of the $2N$ Fourier coefficients X_n of (36) and of the unknowns c_0, U_0' and Ψ_0 is achieved the following way. Wave elevation is sampled during a time T at a frequency F_e. For reasons of computer limitations the records are sliced into blocks containing only K values of the measured surface elevation η_{mk} and the problem is solved separately over each block. Using (A9) to relate U_0' to c_0, this leads to an overdeterminated system of $2K$ equations (15)-(16) with $2N$+2 unknowns. This system is solved by a least squares method minimizing the quadratic error

$$E_T=\frac{1}{K}\sum_{k=1}^{K}\left\{\lambda\left[Q_k-1/K\sum_{k=1}^{K}Q_k\right]^2+\left(\eta_{mk}-\eta_{pk}\right)^2\right\} \tag{B1}$$

In (B1,) Q_k and η_{pk} denote, respectively, the value of the right-hand side of (16) and of the wave elevation evaluated at each sampled point, whereas λ is a Lagrange multiplier to be precised later. The η_{pk} is computed at each iteration by solving (15) with a Newton-Raphson method, whereas data η_{mk} are used in the evaluation of (16). The same procedure is repeated on each block of data. No overlapping between blocks is used because tests show that only prediction of $\tilde{v}_{P2}$ is slightly improved by this technique, whereas no significant effect is found on $\tilde{v}_{P1}$. Since in any case, $\tilde{v}_{P2}$ cannot be very accurately predicted (see the discussion in subsection 3.5), this option was found unnecessary. It is worth noting that owing to the block by block processing, the method does not imply that the wave field conserves its form during a whole record; the Fourier coefficients differ from block to block, allowing slow amplitude modulations.

Table 2. Parameters Used in the Triple Decomposition Method According to Wind Speed U_∞

U_∞, m/s	K	N	Δf, Hz
4.5	256	60	0.195
6.8	256	60	0.195
9.0	384	90	0.130
13.5	512	120	0.098

K is the number of samples per block data; N is the number of Fourier modes; Δf is the resulting frequency resolution.

As shown in subsection 2.4, the linear part $\tilde{v}_{P1}$ of the orbital potential motion is needed for the computation of several correlations. For this purpose, a linear approximation of the method has been developed. This approximation involves exactly the same algorithm, but kinematic and dynamic conditions (15) and (16) are replaced by

$$(\Psi_p)_{z=0}+\eta c_0=\Psi_1 \tag{B2}$$

$$(1-c_0\ U_0'/g)\,\eta+c_0/g\ (\Psi_{p,z})_{z=0}=Q_1 \tag{B3}$$

Both linear and nonlinear methods have been applied to laboratory data resampled at F_e=50 Hz during a time T=512 s. Since the dominant wave frequency decreases when the free-stream wind speed U_∞ increases, the number K of sampling points in each block data is changed with U_∞ so as to keep the number of wave periods recorded during time $T_K=K/F_e$ approximately constant. The frequency resolution Δf is then determined by requiring that it should be equal to the lowest frequency present in each block data or, in other words, $\Delta f=1/T_K$. Concerning the number N of Fourier modes, $N\Delta f$ must be equal to the highest significant gravity wave frequency f_{max}, and we apply the criterium defined by *Jiang et al.* [1990], f_{max}=11.7 Hz. The values of these parameters are reported in Table 2. Finally, in the minimization procedure we use λ=1 as Lagrange multiplier, and convergence is obtained when the relative variation between two successive values of E_T falls below $\varepsilon_T=10^{-2}$.

Acknowledgments. This research was partly supported by the French PAMOS Program under grants n° 91 / ATP / 631 and 92N50 / 0268.

References

Benilov, A. Yu., and B.N. Filyushkin, Application of methods of linear filtration to an analysis of fluctuations in the surface layer of the sea, *Izv. Acad. Sci. USSR Atmos. Oceanic Phys., Engl. transl., 6*, 477-482, 1970.

Benilov, A. Yu., O.A. Kouznetsov, and G.N. Panin, On the analysis of wind wave-induced disturbances in the atmospheric turbulent surface layer, *Boundary Layer Meteorol., 6*, 269-285, 1974.

Cavaleri, O., and S. Zecchetto, Reynolds stresses under wind waves, *J. Geophys. Res., 92* (C4), 3894-3904, 1987.

Cavaleri, O., J.A. Ewing, and N.D. Smith, Measurement of the pressure and velocity field below surface waves, in *Turbulent Fluxes Through* *the Sea Surface, Wave Dynamics, and Prediction*, edited by A. Favre and K. Hasselmann, pp. 257-272, Plenum, New York, 1978.

Cheung, T.K., A study of the turbulent layer in the water at an air-water interface, Ph.D. dissertation, *Tech. Rep. 287*, Dep. of Civ. Eng., Stanford Univ., Stanford, Calif., 1985.

Cheung, T.K., and R.L. Street, Turbulent layers in the water at an air-water interface, *J. Fluid Mech., 194*, 133-151, 1988a .

Cheung, T.K., and R.L. Street, Wave-following measurements in the water beneath an air-water interface, *J. Geophys. Res., 93*(C11), 14,089-14,097, 1988b .

Coantic, M., A. Ramamonjiarisoa, P. Mestayer, F. Resch, and A. Favre, Wind-water tunnel simulation of small-scale ocean-atmosphere interactions, *J. Geophys. Res., 86*(C7), 6607-6626, 1981.

Craik, A.D.D., and S. Leibovich, A rational model for Langmuir circulations, *J. Fluid Mech., 73*, 401-426, 1976.

Dalrymple, R.A., A finite amplitude wave on a linear shear current, *J. Geophys. Res., 79*(30), 4498-4504, 1974.

Dean, R.G., Stream function representation of non linear ocean waves, *J. Geophys. Res., 70*(18), 4561-4572, 1965.

Jiang, J.Y., R.L. Street, and S.P. Klotz, A study of wave-turbulence interaction by use of a nonlinear water wave decomposition technique, *J. Geophys. Res., 95*(C9), 16,037-16,054, 1990.

Kirby, J.T., and T.M. Chen, Surface waves on vertically sheared flows: Approximate dispersion relations, *J. Geophys. Res., 94*(C1), 1013-1027, 1989.

Lake, B.M., and H.C. Yuen, A new model for nonlinear wind waves, 1, Physical model and experimental evidence, *J. Fluid Mech., 88*, 33-62, 1978.

Lamb, H., *Hydrodynamics*, 6th ed., 738 pp., Dover, New York, 1932.

Leibovich, S., The form and dynamics of Langmuir circulations, *Annu. Rev. Fluid Mech., 15*, 391-427, 1983.

Leykin, I.A., M.A. Donelan, and R.H. Mellen, Bispectral analysis of wind waves measured in a laboratory tank, to appear in *Air-Sea Interactions*, M.A. Donelan, W.H. Hui, and W.J. Plant, eds., the University of Toronto Press, Toronto, Canada, 1994.

Longuet-Higgins, M.S., Eulerian and Lagrangian aspects of surface waves, *J. Fluid Mech., 173*, 683-707, 1986.

Longuet-Higgins, M.S., An effect of sidewalls on waves in a wind wave channel, *J. Geophys. Res., 95*(C2), 1765, 1990.

Magnaudet, J., and L. Masbernat, Interactions des vagues de vent avec le courant moyen et la turbulence, *C.R. Acad. Sci. Paris, Sér. 2*, 1461-1466, 1990.

Magnaudet J., and L. Thais, Orbital rotational motion and turbulence below laboratory wind water waves, *J. Geophys. Res.*, this issue.

Peregrine, D.H., Interaction of water waves and currents, *Adv. Appl. Mech., 16*, 9-117, 1976.

Phillips, O.M., *The Dynamics of the Upper Ocean*, 2nd ed., 336 pp., Cambridge University Press, New York, 1977.

Phillips, O.M., and M.L. Banner, Wave breaking in the presence of wind drift and swell, *J. Fluid Mech., 66*, (4), 625-640, 1974.

Ramamonjiarisoa, A., Contribution à l'étude de la structure statistique et des mécanismes de génération des vagues de vent, Thèse d'Etat Univ. de Provence, Aix-Marseille I, Marseilles, France, 1974.

Reynolds, W.C., and A.K.M.F. Hussain, The mechanics of an organized wave in turbulent shear flow., 3, Theoretical model and comparisons with experiments, *J. Fluid Mech., 54*, 263-288, 1972.

Shonting, D.H., A preliminary investigation of momentum flux in ocean waves, *Pure Appl. Geophys., 57*, 149-152, 1964.

Shonting, D.H., Observations of Reynolds stresses in wind waves, *Pure Appl. Geophys., 81*, 202-210, 1970.

Thomas, G.P., Water wave-current interactions: A review, in *Mechanics of Wave-Induced Forces on Cylinders*, edited by T.L. Shaw, pp. 179-203, Pitman, London, 1979.

Thomas, G.P., Wave-current interactions: An experimental and numerical study, 2, Nonlinear waves, *J. Fluid Mech., 216*, 505-536, 1990.

Willert, C.E., and M. Gharib, Digital particle image velocimetry, *Exp. Fluids, 10*, 181-193, 1991.

Wu, J., Wind-induced drift currents, *J. Fluid Mech., 34*, 49-70, 1975.

Yefimov, V.V., and G.N. Khristoforov, Wave-related and turbulent components of velocity spectrum in the top sea layer, *Izv. Acad. Sci. USSR Atmos. Oceanic Phys., Engl. Transl., 7*(2), 200-210, 1971a .

Yefimov, V.V., and G.N. Khristoforov, Spectra and statistical relations between the velocity fluctuations in the upper layer of the seas and surface waves, *Izv. Acad. Sci. USSR Atmos. Oceanic Phys., Engl. Transl., 7*(12), 1290-1310, 1971b .

Yefimov, V.V., Y.U.P Solov'yev, and G.N. Khristoforov, Observational determination of the phase velocities of spectral components of wind waves, *Izv. Acad. Sci. USSR Atmos. Oceanic Phys., Engl. Transl., 8*(4), 1972.

J. Magnaudet and L. Thais, Institut de Mécanique des Fluides de Toulouse, 2 Avenue Camille Soula, 31400 Toulouse, France. (e-mail: magnau@imft.enseeiht.fr; thais@imft.enseeiht.fr)

(Received April 7, 1994; revised October 13, 1994; accepted October 13, 1994.)